MOMENTUM TRANSFER AND TURBULENT KINETIC ENERGY BUDGETS WITHIN A DENSE MODEL CANOPY

D. POGGI
Dipartimento di Idraulica, Trasporti ed Infrastrutture Civili Politecnico di Torino, Torino, Italy & Department of Civil and Environmental Engineering, Duke University, Durham, North Carolina, U.S.A.

G. G. KATUL
Nicholas School of the Environment and Earth Sciences, Duke University, Durham, North Carolina, U.S.A.

J. D. ALBERTSON
Department of Civil and Environmental Engineering, Duke University, Durham, North Carolina, U.S.A.

(Received in final form 8 July 2003)

Abstract. Second-order closure models for the canopy sublayer (CSL) employ a set of closure schemes developed for 'free-air' flow equations and then add extra terms to account for canopy related processes. Much of the current research thrust in CSL closure has focused on these canopy modifications. Instead of offering new closure formulations here, we propose a new mixing length model that accounts for basic energetic modes within the CSL. Detailed flume experiments with cylindrical rods in dense arrays to represent a rigid canopy are conducted to test the closure model. We show that when this length scale model is combined with standard second-order closure schemes, first and second moments, triple velocity correlations, the mean turbulent kinetic energy dissipation rate, and the wake production are all well reproduced within the CSL provided the drag coefficient (C_D) is well parameterized. The main theoretical novelty here is the analytical linkage between gradient-diffusion closure schemes for the triple velocity correlation and non-local momentum transfer via cumulant expansion methods. We showed that second-order closure models reproduce reasonably well the relative importance of ejections and sweeps on momentum transfer despite their local closure approximations. Hence, it is demonstrated that for simple canopy morphology (e.g., cylindrical rods) with well-defined length scales, standard closure schemes can reproduce key flow statistics without much revision. When all these results are taken together, it appears that the predictive skills of second-order closure models are not limited by closure formulations; rather, they are limited by our ability to independently connect the drag coefficient and the effective mixing length to the canopy roughness density. With rapid advancements in laser altimetry, the canopy roughness density distribution will become available for many terrestrial ecosystems. Quantifying the sheltering effect, the homogeneity and isotropy of the drag coefficient, and more importantly, the canonical mixing length, for such variable roughness density is still lacking.

Keywords: Canopy turbulence, Closure models, Cumulant expansion, Drag coefficient, Ejections and sweeps, Mixing length, Nonlocal transport.

Boundary-Layer Meteorology **111:** 589–614, 2004.

1. Introduction

The need to understand and quantify biogeochemical cycles and their role in climate change has sparked substantial interest in canopy turbulence. This interest is perhaps most visible by the proliferation of long-term eddy-flux measurements of carbon dioxide aimed at quantifying the carbon sink in the terrestrial biosphere (Baldocchi et al., 2001). An understanding of the flow within morphologically simple canopies is a necessary first step toward these broader problems (Finnigan, 2000).

The spatial and temporal domains of biosphere-atmosphere exchange problems are on the order of tens of kilometres and several decades, respectively (Katul et al., 2001). Since many of the important scalar transfer problems focus on turbulent fluctuations from the mean state, some information about the statistical structure of the turbulent excursions must be considered. Among the most detailed approaches to simulate turbulent excursions is the large-eddy simulation (LES) technique, in which energetic eddies along with many attributes of the energy cascade are explicitly resolved. LES for canopy flows has progressed significantly over the last decade since the seminal work of Shaw and Schumann (1992) and now offers a promising tool for resolving interactions between landscape heterogeneity and turbulence (Albertson et al., 2001). However, the time scales required for modelling landscape dynamics (e.g., decades) and biogeochemical cycles (e.g., years) far exceed the computational ability of LES, thus necessitating the use of computationally efficient but simpler transport models such as Reynolds averaged closure approaches. The minimum level of complexity needed to describe the distribution of these excursions is second-order closure (Launder, 1996; Hanjalic, 2002; Ayotte et al., 1999).

While second-order closure models were originally developed and have been used for more than 30 years (e.g., Meller, 1973; Lumley, 1978; Launder, 1996; Hanjalic, 2002), their application to canopy turbulence continues to be a major research area. After Wilson and Shaw's (1977) study, numerous second-order closure models for the canopy sublayer (CSL) were proposed (e.g., Meyers and Paw U, 1986; Wilson, 1988; Katul and Albertson, 1998; Massman, 1999; Katul and Chang, 1999; Ayotte et al., 1999) but the reported successes have been mixed (Katul and Albertson, 1998; Katul and Chang, 1999; Pinard and Wilson, 2001). Some of the weaknesses of second-order closure models have been attributed to the inability of eddy-viscosity models to simulate flows subject to forces imposed by bodies immersed in the fluid or flows with significant non-local momentum exchange, as is the case within the CSL (Shaw 1977; Raupach 1988; Wilson 1988; Ayotte et al., 1999; Finnigan, 2000; Hanjalic, 2002). Attempts to rectify these limitations by increasing the closure order have not translated into significantly improved predictive skill (Katul and Albertson, 1998; Hanjalic, 2002). An underlying reason for the inaccuracies is the dependence on a single (and typically local) length scale

to characterize the entire effect of turbulence on the statistical moments being modelled.

Here, we propose a formulation of the mixing length that accounts for the basic energetic modes within the canopy CSL and we embed this within a second-order closure model. Using detailed flume experiments we verify that this approach reproduces well the first and second moments, and even triple velocity correlations. Furthermore, this study demonstrates analytical linkages between standard second-order schemes, large organized structures, and non-local transport inside the canopy via third-order cumulant expansion (CEM). In fact, we show that the incomplete third-order CEM proposed by Katul et al. (1997), when combined with second-order closure principles, quantitatively describes many key statistical attributes of the ejection-sweep cycle within the CSL. The flume experiments used to test the closure model include detailed spatial velocity measurements using non-intrusive laser Doppler anemometry (LDA). The LDA provides velocity statistics near obstacles as well as the channel bottom even when a dense canopy is placed within the flume. These measurements are well suited for assessing how well closure models reproduce terms such as turbulent wake production. However, before discussing these experiments, a brief review of second-order closure models within the CSL is first provided.

2. Theory

Upon time and horizontal averaging the instantaneous momentum equation for non-stratified flows, we obtain:

$$\frac{\partial \langle \overline{u_i} \rangle}{\partial t} + \langle \overline{u_j} \rangle \frac{\partial \langle \overline{u_i} \rangle}{\partial x_j} = -\frac{\partial \langle \overline{p} \rangle}{\partial x_i} + \frac{\partial \tau_{ij}}{\partial x_j} + f_{\mathrm{F,V}}, \tag{1}$$

where

$$\tau_{ij} = -\langle \overline{u_i' u_j'} \rangle - \langle \overline{u_i'' u_j''} \rangle + \nu \frac{\partial \langle \overline{u_i} \rangle}{\partial x_j} \tag{2}$$

and

$$f_{\mathrm{F,V}} = \left\langle \frac{\partial \overline{p''}}{\partial x_i} \right\rangle + \left\langle \nu \frac{\partial^2 \overline{u_i''}}{\partial x_j \partial x_j} \right\rangle. \tag{3}$$

In these expressions, t is time, x_i ($x_1 = x, x_2 = y, x_3 = z$) are the longitudinal, lateral, and vertical directions, respectively; u_i ($u_1 = u, u_2 = v, u_3 = w$) are the instantaneous velocity components along x_i; p is the static pressure normalized by the mean fluid density; and ν is the kinematic viscosity. All flow variables are decomposed into temporal and planar averages with turbulent excursions defined

from the time-averaged (denoted by overbar) and horizontally-averaged (denoted by angular brackets) quantities using the convention in Raupach and Shaw (1982) and Finnigan (1985, 2000). That is,

$$\phi_j = \overline{\phi_j} + \phi'_j, \tag{4a}$$

$$\overline{\phi_j} = \langle \overline{\phi_j} \rangle + \overline{\phi''_j}. \tag{4b}$$

All double primed terms arise because horizontal averaging and differentiation do not commutate for the multiply-connected air spaces within the vegetation. Hence, they represent the explicit effects of the vegetation on the spatial and temporal statistics of the flow. These terms contain the drag force $f_{\mathrm{F,V}}$, which is composed of form and viscous drag terms. The stress tensor τ_{ij} also contains the conventional turbulent and viscous stresses and a dispersive flux term $\langle \overline{u''_i u''_j} \rangle$ resulting from spatial correlations in the time-averaged velocity field. Using the same averaging procedures, the second-moment equations are given by

$$\begin{aligned}
\left(\frac{\partial}{\partial t} + \langle \overline{u_j} \rangle \frac{\partial}{\partial x_j}\right) \langle \overline{u'_i u'_k} \rangle \;=\; & -\left(\langle \overline{u'_j u'_k} \rangle \frac{\partial \langle \overline{u_i} \rangle}{\partial x_j} + \langle \overline{u'_i u'_j} \rangle \frac{\partial \langle \overline{u_k} \rangle}{\partial x_j} \right) \\
& - \frac{\partial \langle \overline{u''_j u_i u''_k} \rangle}{\partial x_j} - \left(\left\langle \overline{u'_j u'_k}'' \frac{\partial \overline{u_i}''}{\partial x_j} \right\rangle + \left\langle \overline{u'_i u'_j}'' \frac{\partial \overline{u''_k}}{\partial x_j} \right\rangle \right) \\
& - \frac{\partial \langle \overline{u'_i u'_j u'_k} \rangle}{\partial x_j} - \left(\left\langle \frac{\partial \overline{p' u'_i}}{\partial x_k} \right\rangle + \left\langle \frac{\partial \overline{p' u'_k}}{\partial x_i} \right\rangle \right) \\
& + \nu \frac{\partial^2 \langle \overline{u'_i u'_k} \rangle}{\partial x_j \partial x_j} + \left\langle \overline{p' \left(\frac{\partial u'_i}{\partial x_k} + \frac{\partial u'_k}{\partial x_i} \right)} \right\rangle - 2\nu \left\langle \overline{\frac{\partial u'_i}{\partial x_j} \frac{\partial u'_k}{\partial x_j}} \right\rangle.
\end{aligned} \tag{5}$$

The closure parameterizations for the triple velocity moments, the mean turbulent kinetic energy dissipation rate, the pressure-velocity interaction, and the effect of the canopy on the flow field are discussed next.

2.1. THE CLOSURE SCHEMES

The closure approximations we adopted are those of Wilson and Shaw (1977), which we repeat for completeness. We chose this model because (i) it explicitly links the closure schemes to an empirical mixing length, (ii) it is the most parsimonious among the numerous second-order closure models proposed, and (iii) it is the most cited canopy second-order closure model to date. For the mean momentum equation, the closure approximations are:

$$\left\langle \frac{\partial \overline{p}''}{\partial x_i} \right\rangle = C_d \, a \, \langle |\overline{u}| \rangle \langle \overline{u}_i \rangle, \tag{6a}$$

$$\nu\left\langle\frac{\partial^2\overline{u}_i''}{x_j\,x_j}\right\rangle\approx 0, \tag{6b}$$

where $|u|$ is the magnitude of the velocity. Such an approximation assumes that the form drag by the canopy on the fluid can be modelled as a general drag force characterized by a drag coefficient (C_d) and a local canopy density (a). Also, the viscous drag was neglected relative to the general drag force.

For the Reynolds stresses, the closure approximations include the following (Mellor, 1973; Wilson and Shaw, 1977). For the transport terms

$$P_T=\left(\left\langle\frac{\partial\overline{p'u_i'}}{\partial x_k}\right\rangle+\left\langle\frac{\partial\overline{p'u_k'}}{\partial x_i}\right\rangle\right)+\frac{\partial}{\partial x_j}\langle\overline{u_i'u_j'u_k'}\rangle, \tag{7}$$

the standard gradient-diffusion model is adopted

$$P_T=-\frac{\partial}{\partial x_j}\left(q\lambda_1\left(\frac{\partial\langle\overline{u_i'u_j'}\rangle}{\partial x_k}+\frac{\partial\langle\overline{u_i'u_k'}\rangle}{\partial x_j}+\frac{\partial\langle\overline{u_j'u_k'}\rangle}{\partial x_i}\right)\right), \tag{8}$$

where $q=\sqrt{\langle\overline{u_i'u_i'}\rangle}$ is the turbulent velocity scale, and λ_1 is a characteristic length scale for the triple velocity correlation. Here, we neglected the dispersive transport terms. Several wind-tunnel experiments suggest that such dispersive transport terms are small (Finnigan, 2000).

The expansion of pressure velocity correlation, along with the return to isotropy closure approximation, leads to:

$$\begin{aligned}\left(\left\langle\overline{p'\frac{\partial u_j'}{\partial x_i}}\right\rangle+\left\langle\overline{p'\frac{\partial u_i'}{\partial x_j}}\right\rangle\right) &= -q\lambda_2\left[\langle\overline{u_i'u_j'}\rangle-\delta_{ij}\frac{q^2}{3}\right]\\ &\quad +Cq^2\left[\frac{\partial\langle\overline{u}_i\rangle}{\partial x_j}+\frac{\partial\langle\overline{u}_j\rangle}{\partial x_i}\right],\end{aligned}$$

where λ_2 is a characteristic length scale of the velocity-pressure correlation, and C is a closure constant to be determined. The viscous dissipation is modelled as a function of the available turbulent kinetic energy, and is given by

$$2\nu\left\langle\overline{\frac{\partial u_i'}{\partial x_j}\frac{\partial u_k'}{\partial x_j}}\right\rangle=\frac{2}{3}\frac{q^3}{\lambda_3}\delta_{ik}, \tag{9}$$

where λ_3 is a dissipation length scale.

When the dispersive fluxes are negligible, as expected in dense canopies (e.g., Finnigan, 2000; Poggi et al., 2003b), the wake production terms are given by

$$-\left\langle\overline{u_i'u_j'}''\frac{\partial\overline{u}_i''}{\partial x_j}\right\rangle=\langle\overline{u}_i\rangle\left\langle\frac{\partial\overline{p}''}{\partial x_i}\right\rangle, \tag{10}$$

as shown in Raupach and Shaw (1982). Based on the Wilson and Shaw (1977) closure models, these terms can be expressed as

$$-\left\langle \overline{u_i' u_j'}'' \frac{\partial \overline{u}_i''}{\partial x_j} \right\rangle = \langle \overline{u_i} \rangle \, C_d \, a \, \langle \overline{u_i} \rangle^2. \tag{11}$$

The present closure model is an over simplification of the energetic pathway when compared to more recent closure models (e.g., Wilson, 1988; Ayotte et al., 1999) as the TKE is not explicitly split into large-scale (SKE) and wake-scale (WKE) bands.

2.2. THE CSL SECOND-ORDER CLOSURE MODEL

Upon replacing the above closure approximations into the mean momentum and Reynolds stress equations, assuming a stationary and planar-homogeneous flow, and neglecting all the dispersive fluxes, the standard second-order closure model of Wilson and Shaw (1977) for CSL turbulence reduces to (in meteorological notation):

$$\langle \overline{u} \rangle : \quad \frac{\partial \langle \overline{u'w'} \rangle}{\partial z} + C_d \, a \, \langle \overline{u} \rangle^2 = 0, \tag{12}$$

$$\langle \overline{u'w'} \rangle : \quad -\langle \overline{w'^2} \rangle \frac{d\langle \overline{u} \rangle}{dz} + 2\frac{d}{dz}\left(q\lambda_1 \frac{d\langle \overline{u'w'} \rangle}{dz} \right) - q\frac{\langle \overline{u'w'} \rangle}{3\lambda_2} - Cq^2 \frac{d\langle \overline{u} \rangle}{dz} = 0, \tag{13}$$

$$\begin{aligned} \langle \overline{u'u'} \rangle : \quad & -2\langle \overline{u'w'} \rangle \frac{d\langle \overline{u} \rangle}{dz} + \frac{d}{dz}\left(q\lambda_1 \frac{d\langle \overline{u'u'} \rangle}{dz} \right) + 2C_d a \langle \overline{u} \rangle^3 \\ & -\frac{q}{3\lambda_2}\left(\langle \overline{u'u'} \rangle - \frac{q^2}{3} \right) - \frac{2}{3}\frac{q^3}{\lambda_3} = 0, \end{aligned} \tag{14}$$

$$\langle \overline{v'v'} \rangle : \quad \frac{d}{dz}\left(q\lambda_1 \frac{d\langle \overline{v'v'} \rangle}{dz} \right) - \frac{q}{3\lambda_2}\left(\langle \overline{v'v'} \rangle - \frac{q^2}{3} \right) - \frac{2}{3}\frac{q^3}{\lambda_3} = 0, \tag{15}$$

$$\langle \overline{w'w'} \rangle : \quad \frac{d}{dz}\left(q\lambda_1 \frac{d\langle \overline{w'w'} \rangle}{dz} \right) - \frac{q}{3\lambda_2}\left(\langle \overline{w'w'} \rangle - \frac{q^2}{3} \right) - \frac{2}{3}\frac{q^3}{\lambda_3} = 0. \tag{16}$$

It is common to express the three length scales λ_1, λ_2, and λ_3 as a function of one principle length scale using (Wilson and Shaw, 1977; Katul and Albertson, 1998)

$$\lambda_i = b_i \, l_{\text{eff}}; \quad i = 1, 2, 3 \tag{17}$$

where b_i are closure coefficients, and l_{eff} is the effective (or principle) length scale of the closure model. This length scale is central to the accuracy of the closure

model calculations and is the subject of sub-Section 5.2. To solve for the flow statistics within the CSL using the above set of equations, appropriate boundary conditions, the parameters l_{eff}, C_d, and a, as well as the four closure constants $b_i (i = 1, 2, 3)$ and C must be determined or specified. Given that the characteristic velocity (q) and l_{eff} in the closure model are intimately linked with the turbulent kinetic energy (TKE), we consider how the standard closure assumptions affect the individual components of the TKE budget.

2.3. The turbulent kinetic energy budget

With the above closure approximations, the components of the turbulent kinetic energy (TKE) budget reduce to:

$$0 = P_s + P_w + P_T + P_d, \tag{18}$$

where P_s, P_w, P_t, and P_d are the shear production, wake production, turbulent transport, and viscous dissipation rates, respectively, and are given by:

$$P_s = -2\langle\overline{u'w'}\rangle \frac{d\langle\overline{u}\rangle}{dz}, \tag{19}$$

$$P_w = 2C_d a \langle\overline{u}\rangle^3, \tag{20}$$

$$P_t = \frac{d}{dz}\left(q\lambda_1\left[\frac{d\langle\overline{u'u'}\rangle}{dz} + \frac{d\langle\overline{v'v'}\rangle}{dz} + \frac{d\langle\overline{w'w'}\rangle}{dz}\right]\right), \tag{21}$$

$$P_d = -2\frac{q^3}{\lambda_3}. \tag{22}$$

The TKE budget will serve as a benchmark, by assessing how well the closure model reproduces the measured P_s, P_w, P_d, and P_t.

2.4. Non-local transport and second-order closure models

As earlier stated, one of the main criticism of second-order closure models is their failure to simulate non-local momentum exchange within the CSL (see Katul and Albertson, 1998). Here, we associate non-local momentum transport with large-scale vortical motion that is produced elsewhere in the flow domain but contributes to the local Reynolds stress at a given layer. Hence, it is constructive to assess how well this closure model reproduces the measured effects of these non-local transport phenomena, such as the ejection-sweep cycle, on the local momentum flux when a realistic l_{eff} is employed. The ejection-sweep cycle is typically quantified via conditional sampling methods and quadrant analysis, as reviewed in Antonia (1981). Quadrant analysis refers to the joint scatter of two turbulent quantities (e.g.,

w' and u'). The four quadrants defined by the cartesian plane (abscissa is u' and ordinate is w') reflects four modes of momentum transfer: quadrant 1 for which $u' > 0$ and $w' > 0$ is commonly labeled as the outward interaction quadrant, quadrant 2 for which $u' < 0$ and $w' > 0$ is dominated by ejections, quadrant 3 for which $u' < 0$ and $w' < 0$ is often labeled as the inward interaction quadrant, and quadrant 4 for which $u' > 0$ and $w' < 0$ is dominated by sweeps. Nakagawa and Nezu (1977) and Raupach (1981) showed that the difference in stress fractions (ΔS_o), given by

$$\Delta S_o = \frac{\langle\overline{w'u'}\rangle|_4 - \langle\overline{w'u'}\rangle|_2}{\langle\overline{u'w'}\rangle} \tag{23}$$

is connected with ejections and sweeps, where $\langle\overline{w'u'}\rangle|_i/\langle\overline{u'w'}\rangle$ is the stress fraction in quadrant i ($i = 1, 2, 3, 4$). To link ΔS_o with second-order closure models, we build on the pioneering work of Nakagawa and Nezu (1977) and Raupach (1981) in which the third-order cumulant expansion method (CEM) was proposed and successfully used. For example, Raupach (1981) demonstrated that:

$$\Delta S_o = \frac{(R_{uw}+1)}{R_{uw}\sqrt{2\pi}}\left[\frac{2C_1}{(1+R_{uw})^2} + \frac{C_2}{1+R_{uw}}\right], \tag{24}$$

where R_{uw}, C_1, and C_2 are given by

$$\begin{aligned}
R_{uw} &= \frac{\langle\overline{w'u'}\rangle}{\sigma_u\sigma_w},\\
C_1 &= \left(1+R_{uw}\right)\left[\frac{1}{6}(M_{03}-M_{30}) + \frac{1}{2}(M_{21}-M_{12})\right],\\
C_2 &= -\left[\frac{1}{6}(2-R_{uw})(M_{03}-M_{30}) + \frac{1}{2}(M_{21}-M_{12})\right],\\
M_{ab} &= \frac{\langle\overline{w'^a u'^b}\rangle}{\sigma_w^a\sigma_u^b}; \quad \sigma_s = \sqrt{\langle\overline{s's'}\rangle},
\end{aligned}$$

where σ_s is the time and horizontally averaged standard deviation of any flow variable s. After demonstrating that the mixed moments M_{12} and M_{21} contribute much more to ΔS_o than M_{03} and M_{30}, Katul et al. (1997) suggested a further simplification given by

$$\Delta S_o \approx \frac{1}{2R_{uw}\sqrt{2\pi}}\left[M_{21} - M_{12}\right] \tag{25}$$

hereafter referred to as an incomplete CEM (ICEM). Using the gradient-diffusion approximations for $\langle\overline{w'u'w'}\rangle$ and $\langle\overline{w'u'u'}\rangle$ along with the ICEM, and after algebraic manipulations, the second-order closure model prediction for ΔS_o reduces to:

$$\Delta S_o = \frac{-1}{2\sqrt{2\pi}}\frac{q\lambda_1}{\langle\overline{w'u'}\rangle}\left[\frac{1}{\sigma_u}\frac{\partial\langle\overline{u'u'}\rangle}{\partial z} - \frac{2}{\sigma_w}\frac{\partial\langle\overline{w'u'}\rangle}{\partial z}\right]. \tag{26}$$

Comparison between measured and modelled ΔS_o from Equation (26) provides an explicit evaluation of how well second-order closure models reproduce the stress fraction contribution of ejections and sweeps. Given that the contribution to momentum transfer of ejections and sweeps is non-local, such ΔS_o comparison serves as an independent benchmark of how well second-order closure models capture non-local transport phenomena in the CSL.

3. Experimental Setup

Much of the experimental setup is described in Poggi et al. (2004a); however, a brief review is provided for completeness. The experiment was conducted at the hydraulics Laboratory, DITIC Politecnico di Torino, in a re-circulating flume whose main component is a rectangular channel 18 m long, 0.90 m wide and 1 m high. The model canopy is composed of an array of vertical rustproof steel cylinders 120 mm high ($= h$), and 4 mm in diameter ($= d_r$) arranged in a regular pattern along the 9 m long and 0.9 m wide test section. The frontal area index (λ_{FAI}) is 1072 rods m^{-2}. As discussed later, this frontal area index leads to a drag coefficient comparable to drag estimates reported for dense forested ecosystems with leaf area index (LAI) ranging from 3.5 to 6 (Katul and Albertson, 1998).

The water velocity was measured by two-component laser Doppler anemometry (LDA) employed in a forward scattering mode. An advantage of LDA is its small averaging volume, its non-intrusive nature, and its ability to measure water velocities close to the cylinders and channel bottom. In this study, a measurement run consists of sampling the u and w time series at a particular position between the rods. Given the spatial non-homogeneity in the flow statistics, 11 measurement locations were used. These 11 locations were unevenly spaced between the rods; locations were chosen such that sampling was densest within regions in which the flow statistics exhibit the highest spatial variability. In Figure 1, the plan view of the locations of the cylinders and the sampling positions are shown along with the representative area used to weight each measurement position. At each of the 11 positions, we collected 15 runs in the vertical (see Figure 1). The sampling duration and frequency were 300 s and 2500–3000 Hz, respectively.

The experiments were conducted at two very high Reynolds numbers differing by a factor of about 1.5 to further quantify whether the closure schemes and constants are overly sensitive to the Reynolds number variations (Pope, 2000). Using the vertically-averaged velocity (U_b) across the entire water depth (h_w), the resulting bulk Reynolds number Re_b ($= U_b h_w/\nu$) for the two experiments are 116,560 and 172,300, which ensures fully-developed turbulent flows in both cases.

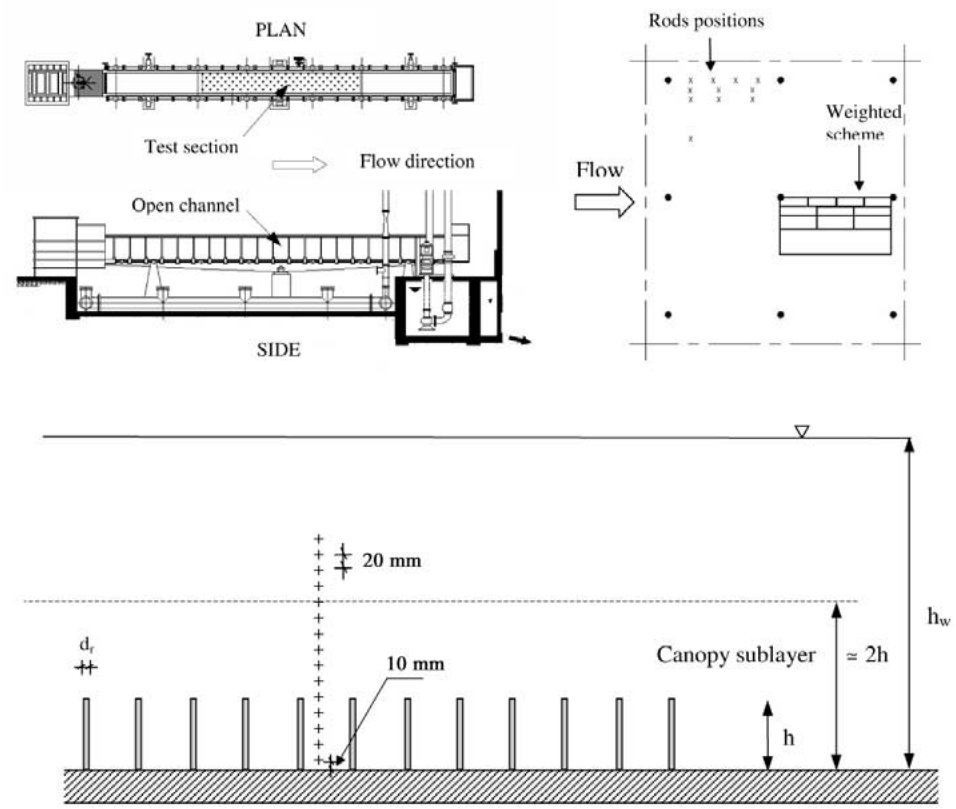

Figure 1. A view of the three hierarchical scales of the experiment: The channel flow facility and the working section (top left), the plan view of the spatial sampling points and their area-weighted contribution to spatial averaging (top right), and the section view of the measurement locations in relation to the canopy dimensions (bottom).

4. Data Analysis

Before comparing measured and modelled quantities, a brief description on how the measurements were used or processed to arrive at statistics that can be compared with the time and planar-averaged closure model calculations is discussed.

4.1. Measurements of the statistical moments

When computing the measured statistical moments and their vertical profiles, we first time averaged and then planar-averaged the quantities, in keeping with the averaging procedures described in Raupach and Shaw (1982). The planar averaging at each vertical position was performed using a weighted scheme, with weights proportional to the fraction of total ground area represented by each position as shown in Figure 1. The statistics that are explicitly considered in model comparisons with

measurements include: $\langle\overline{u}\rangle$, $\langle\overline{u'w'}\rangle$, $\langle\overline{u'u'}\rangle$, $\langle\overline{w'w'}\rangle$, $\langle\overline{w'u'u'}\rangle$, $\langle\overline{w'u'w'}\rangle$, $\langle\Delta S_o\rangle$, P_s, and P_t. With spatial time series data we can directly estimate key components of the TKE budget such as P_w, which are difficult to estimate in atmospheric field experiments.

4.2. Measurements of wake production and TKE dissipation

In the temporally and spatially averaged Reynolds stress equation, and in the absence of dispersive fluxes, the wake production of turbulent kinetic energy is given by Raupach and Shaw (1982); Finnigan (2000); Ayotte et al. (1999)

$$P_w = -\left\langle \overline{u_i'u_k'}'' \frac{\partial \overline{u_i}''}{\partial x_k} + \overline{u_i'u_k'}'' \frac{\partial \overline{u_i}''}{\partial x_k} \right\rangle, \tag{27}$$

which, for a planar homogeneous flow, reduces to

$$P_w = -\left\langle 2\overline{u'w'}'' \frac{\partial \overline{u}''}{\partial z} \right\rangle. \tag{28}$$

With this estimate, an explicit comparison between modelled and measured P_w is now possible. Naturally, the limited spatial sampling of the velocity produces large uncertainties in the measured P_w; hence, agreement between measured and modelled P_w may in fact provide added confidence in the spatial sampling scheme proposed in Figure 1.

Furthermore, independent estimates of P_d are possible from our experimental data using the isotropic relation

$$P_d = -15\nu\left\langle \overline{\left(\frac{\partial u}{\partial x}\right)^2} \right\rangle. \tag{29}$$

We chose this method of estimating the dissipation rate because it is entirely independent of the TKE budget. However, care should be used when quantitatively comparing the second-order closure model calculations with these estimates. This, in part, is due to the fact that (i) Taylor's hypothesis is used to estimate the spatial derivatives from temporal derivatives in high intensity flows, and (ii) the local dissipation by wakes is only partly accounted for. Nonetheless, the canonical shape and order of magnitude estimates by this dissipation method are valuable in 'first order magnitude' comparisons between measured and modelled dissipation rates, given the limited dissipation measurements reported in the CSL.

5. Closure Model Parameterization

As stated earlier, to solve for the flow statistics by the second-order closure model, parameters l_{eff}, C_d, and a, as well as the four closure constants b_i ($i = 1, 2, 3$) and C must be determined or specified. In this section, we discuss their estimation and parameterization.

5.1. Estimation of the drag coefficient

To estimate C_d, we use the mean momentum equation, given by

$$C_D = -\left(\frac{\partial\langle\overline{u'w'}\rangle}{\partial z} + \frac{\partial\langle\overline{p}\rangle}{\partial x}\right)\left(a\,\langle\overline{u}\rangle^2\right)^{-1} \tag{30}$$

along with the measured $\partial\langle\overline{p}\rangle/\partial x$ and profiles of $\langle\overline{u'w'}\rangle$ and $\langle\overline{u}\rangle$ from a wide range of experiments conducted in this flume for the same rod type (but different canopy density) described in Poggi et al. (2004a). When all C_D values are combined from these experiments and plotted as a function of the element Reynolds number Re_d ($= \langle\overline{u}\rangle\, d_r/\nu$) in Figure 2, a clear relationship emerges. This relationship can be approximated by (Poggi et al., 2004a)

$$C_D \approx \frac{1}{2}\left[1.5 - 8.5\times 10^{-4}\,\text{Re}_d\right]. \tag{31}$$

At low Reynolds numbers, the C_D is consistent with the classical behaviour of drag on a unit length of an isolated cylinder (i.e., $C_D \simeq \text{Re}_d^{1/2}$; Bachelor, 1967). With increasing Reynolds number, the C_D values monotonically decrease (rather than attain a constant value, as is the case for an isolated cylinder). This decrease is generally attributed to the sheltering effect (Raupach and Thom, 1981; Raupach, 1994; Massman, 1997). Interestingly, the computed values are in agreement with several observed drag coefficients reported in situ and in some wind-tunnel studies (Thom, 1971; Seginer, 1976; Brunet et al., 1994; Raupach et al., 1996). An immediate consequence here is that C_D can be fully described by Re_d. This approach is adopted in our closure model calculations; however, we acknowledge that this relationship requires further testing for other canopy configurations before any universality should be inferred.

5.2. Estimation of the principle length scale

The length scale adopted in our closure model is based on the canonical structure of turbulence inside and just above the canopy as described by Poggi et al. (2004a). In Poggi et al. (2004a), it was demonstrated that the effective length scale is dominated by three fundamental length scales: rod diameter (d_r), the shear length scale

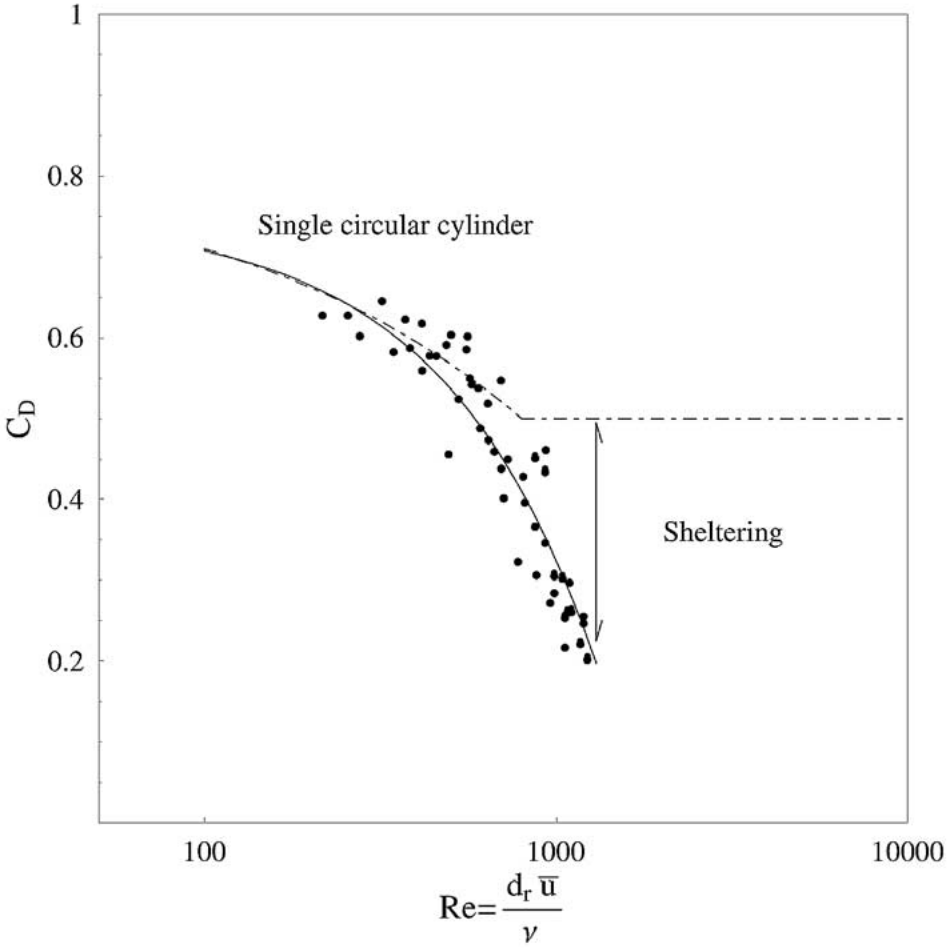

Figure 2. Variation of the measured drag coefficient (C_D) with element Reynolds number $\mathrm{Re}_d = d_r\langle\overline{u}\rangle/\nu$ across all heights and for 5 canopy densities ranging from sparse (67 rods m^{-2}) to dense (1072 rods m^{-2}).

($L_s = (\overline{u}(\mathrm{d}\overline{u}/\mathrm{d}z)^{-1})_{z=h}$), and distance from the wall (z). It was also demonstrated that the relative importance of these three length scales varies with z/h and λ_{FAI}. For completeness, we briefly review the key arguments in Poggi et al. (2004a).

Inside the canopy ($z/h < 0.5$), hereafter referred to as Region I, flow visualization and spectral measurements demonstrate that the turbulence is primarily produced by small vortices associated with von Karman streets. Near the canopy top ($0.5 < z/h < 1.5$), hereafter referred to as Region II, the length scale was shown to be a superposition of a mixing layer length scale, l_{ML}, and a boundary-layer length scale, l_{BL}. We emphasize that these two vortical motions do not coexist in space, rather, the flow oscillates between one of these two states. Finally, for $z/h > 1.5$, hereafter referred to as Region III, the primary length scale collapses

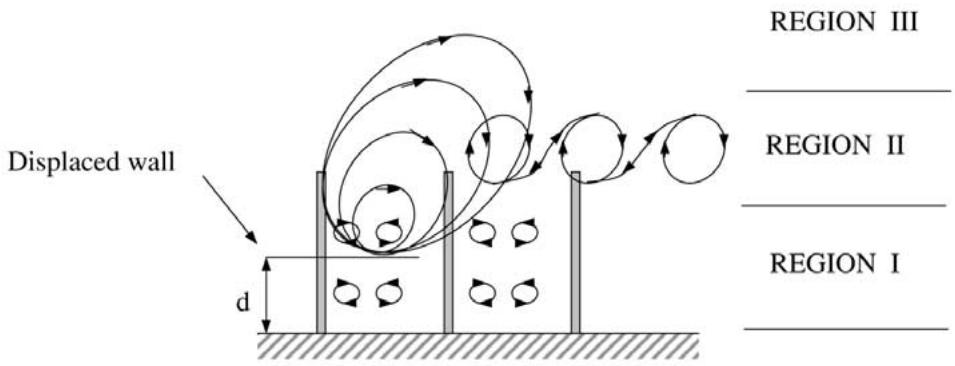

Figure 3. Conceptual model for the mixing length (l_{eff}) within the three regions of the CSL. Region III is dominated by boundary-layer flows, Region II is a mixing layer superimposed on a boundary layer, and Region I is dominated by von Karman streets introduced by the rod diameter d_r.

to the classical displaced boundary-layer length scale $l_{BL} = k(z - d)$, where d is the zero-plane displacement height. An estimate of d can be obtained by the centre-of-pressure method (Thom, 1971; Jackson, 1981)

$$d = \frac{\int_0^h z f_{F,V}(z)\mathrm{d}z}{\int_0^h f_{F,V}(z)\mathrm{d}z}. \tag{32}$$

Hence, the l_{eff} in our second-order closure model takes on the following mathematical form for the different regions (see Figure 3). For Region III, the effective length scale is identical to the standard boundary-layer length scale (l_{BL}) given by

$$l_{\text{eff}} = l_{BL} = k(z - d), \tag{33}$$

where $k = 0.4$ is the Von Karman constant. For Region I, l_{eff} is a constant, independent of the distance from ground surface, and is given by:

$$l_{\text{eff}} \approx l_V = \frac{\langle\overline{u}\rangle}{f} = \left(\frac{d_r}{0.21}\right), \tag{34}$$

where l_V is the mean size of the von Karman street vortex. The value 0.21 is derived from the Strouhal number ($= f d_r/\langle\overline{u}\rangle$) linking frequency of periodic vortices (f) to the mean velocity and the characteristic length scale of the obstacle (in this case d_r). The Strouhal number is approximately constant across a wide range of element Reynolds numbers ($d_r\,\overline{u}/\nu = 60$ to 5000, Schlichting, 1979) suggesting that the 0.21 value will hold for CSL flows. More important, Poggi et al. (2004a) demonstrated that this length scale appears independent of λ_{FAI} and z/h.

In Region II, the flow field is a superposition of the classical surface layer and a perturbed mixing layer. A linear superposition model for the mixing length was proposed by Poggi et al. (2004a) and is given by

$$l_{\text{eff}} = (1 - \alpha) l_{BL}(z) + \alpha(l_{ML}), \tag{35}$$

where α changes from 0 (for a very sparse canopy) to 1 (pure mixing layers) depending on the canopy density. The mixing layer length l_{ML} can be well approximated by

$$l_{ML} = \frac{\langle \overline{u} \rangle}{d\langle \overline{u} \rangle / dz}\bigg|_{z=h} \approx \frac{1}{\widehat{C_D a}} \left(\frac{u_*}{\langle \overline{u} \rangle} \right)^2, \tag{36}$$

where $\widehat{c}$ is the depth-averaged value of a variable c across h as discussed in Poggi et al. (2004a). For dense canopies, both $u_*/\langle \overline{u} \rangle$ and α saturate and become approximately independent of λ_{FAI}, with typical values of 0.3 (Raupach, 1994) and 0.5, respectively. That is, for dense canopies, l_{eff} for Region II simplifies to

$$l_{\mathrm{eff}} \approx 0.5 \left[l_{BL}(z) + \frac{1}{9} \frac{1}{\widehat{C_d a}} \right], \tag{37}$$

which completes the description of the mixing length formulation employed in our second-order closure model calculations for all three regions.

5.3. Estimation of the closure constants and boundary conditions

The closure constants b_i ($i = 1, 2, 3$) and C are generally dependent on the boundary conditions. We first discuss the boundary conditions then proceed to show how the closure constants are computed. The upper boundary condition is set at the point where the observed Reynolds stress departs from linearity and approaches zero ($z/h \simeq 2.8$). At this height, the second-order closure model is assumed to reproduce standard similarity scaling:

$$\frac{d\sigma_u}{dz} = 0, \tag{38a}$$

$$\frac{d\sigma_w}{dz} = 0, \tag{38b}$$

$$\frac{dq}{dz} = 0, \tag{38c}$$

$$\frac{d\langle \overline{u} \rangle}{dz} = \frac{u_*}{k(z-d)}. \tag{38d}$$

For the Reynolds stress, we assumed that $\langle \overline{u'w'} \rangle = 0$ at $z = h_w$. These are the most general boundary conditions that do not require 'data-specific' values for σ_u, σ_w, and q. The lower boundary conditions are not specified at the wall; rather they are specified as a limit with $z/h \ll 1$ and are given by

$$\sigma_u = 0, \quad \sigma_w = 0, \quad \langle \overline{u} \rangle \approx \sqrt{\frac{-\partial \langle \overline{p} \rangle / \partial x}{C_d a}}, \quad \langle \overline{u'w'} \rangle = 0.$$

We chose this boundary condition because the observed mean velocity near the wall is finite. To determine the closure constants (b_1, b_2, b_3, and C), we use the approach of Katul and Albertson (1998) and set $P_s = P_d$ (i.e., local equilibrium) and neglect all flux-transport terms at $z/h = 2.8$ so that

$$b_2^{-1}\left(A_w - \frac{q^2}{3}\right) + b_3^{-1}(2A_q^2) = 0, \tag{39a}$$

$$b_2^{-1}\left(A_u - \frac{q^2}{3}\right) + b_3^{-1}(2A_q^2) = \frac{6}{A_q}, \tag{39b}$$

$$b_2^{-1}\left(\frac{1}{3A_q}\right) + C = \left(\frac{A_w}{A_q}\right)^2, \tag{39c}$$

$$b_1 = \frac{1}{A_q}, \tag{39d}$$

where $\dfrac{\sigma_u}{u_*} = A_u$, $\dfrac{\sigma_w}{u_*} = A_w$, $\dfrac{q}{u_*} = A_q$.

From the experiments, we use for both Re_b cases $A_u = 1.5$, $A_w = 1.2$, $A_q = 2.34$. Hence, the precise values of A_u, A_w, A_q are imposed on the closure constants rather than on the boundary conditions. Solving the above algebraic equations specifies all the needed closure constants for the model calculations.

6. Second-Order Closure Model Testing

Having presented the parameterization of the model, we proceed to the comparisons with the experiments for the two Re_b values. When comparing to the measurements, we use four metrics: (1) First and second moments of the flow field, (2) triple moments, (3) TKE budget, and (4) ΔS_o. The first comparison is to diagnose how well the second-order closure model reproduces the statistics typically needed in scalar transport calculations, the second comparison permits direct assessment as to whether gradient-diffusion approximations are reasonable within the CSL given our proposed l_{eff}, the third comparison offers additional insights about the closure model performance through the wake production term, and the fourth comparison assesses how well the closure model reproduces certain features of the non-local momentum transport associated with the ejection-sweep cycle.

6.1. First- and second-moment comparisons

We show the comparison between measured and modelled $\langle\overline{u}\rangle$, $\langle\overline{u'w'}\rangle$, $\langle\overline{u'u'}\rangle$, $\langle\overline{w'w'}\rangle$ for the two Re_b in Figure 4. A quantitative comparison between measured

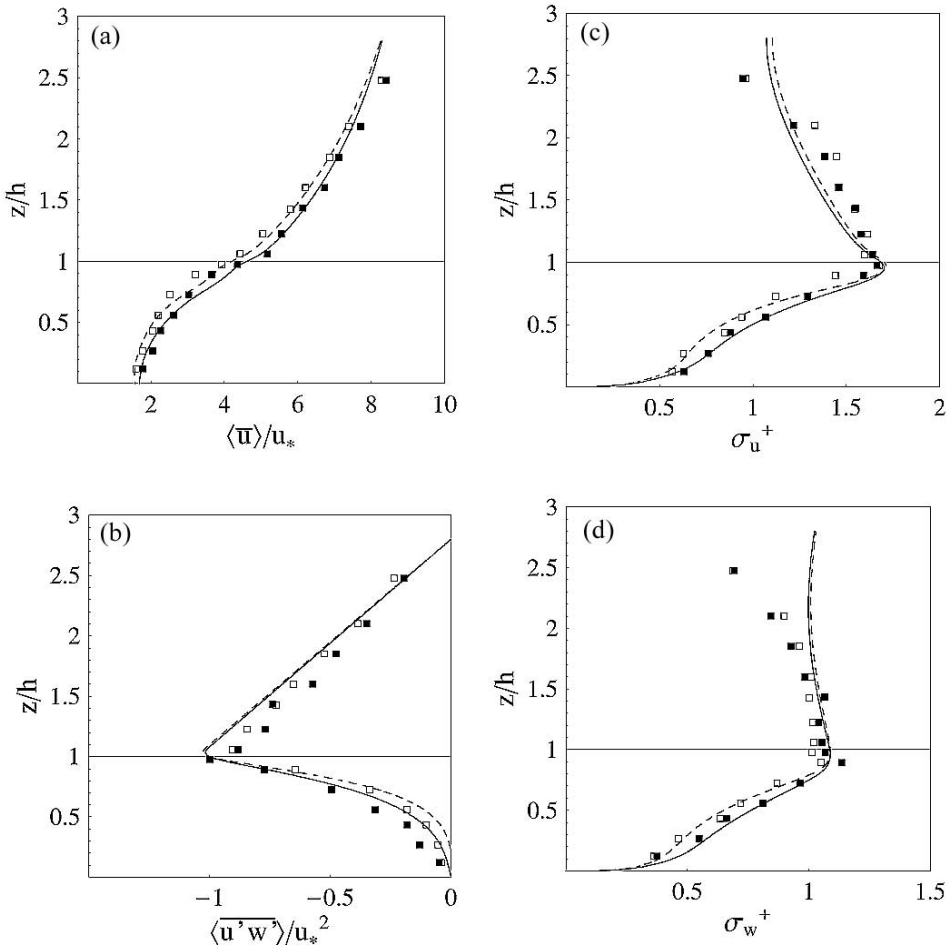

Figure 4. Comparison between measured and modelled horizontally-averaged moments with normalized height (z/h) for (a) mean longitudinal velocity $\langle\overline{u}\rangle/u_*$, (b) mean shear stress $\langle\overline{w'u'}\rangle/(u_*^2)$, (c) mean longitudinal velocity standard deviation $\sigma_u^+ = \sigma_u/u_*$, (d) mean vertical velocity standard deviation $\sigma_w^+ = \sigma_w/u_*$. The solid symbols (measurements) and solid lines (model calculations) are for Re_b = 172,300 while the open symbols (measurements) and dashed lines (model calculations) are for Re_b = 116,560.

and modelled flow statistics is presented in Table I. It is clear that the model reproduces well the first and second moments irrespective of Re_b (for high Re_b). The agreement between measurements and model calculation lends confidence to the formulation of the mixing length and the C_D parameterization because $\langle\overline{u'u'}\rangle$ and $\langle\overline{w'w'}\rangle$ are entirely independent of the mean momentum balance, which was used to estimate C_D.

To place these results in the context of 'real-world' canopies, we compare the model performance for this flume experiment with second- and third-order closure

TABLE I

Comparison between measured and modelled flow statistics. The model evaluation is conducted by regressing measured (independent) upon modelled (dependent) flow variable. The regression slope (a) and intercept (b), the correlation coefficient (r), and the root-mean-squared error ($RMSE$) are presented for both Reynolds number runs. For reference, we show the second- and third-order model comparisons reported in Katul and Albertson (1998) for a 15-year old pine forest. The closure formulations used by Katul and Albertson (1998) are primarily based on the Wilson and Shaw (1977) model.

Re_b	172,300				116,560			
	a	b	r	RMSE	a	b	r	RMSE
$\overline{u}/u_*$	1.04	−0.43	1.00	0.33	1.02	−0.44	0.99	0.40
σ_u^+	1.04	−0.05	0.96	0.09	0.97	0.04	0.95	0.12
σ_w^+	1.08	−0.14	0.92	0.11	0.91	0.02	0.94	0.10
$\frac{\overline{u'w'}}{u_*^2}$	0.84	−0.06	0.99	0.07	0.87	−0.05	0.99	0.06
$\frac{\langle w'u'u'\rangle}{u_*^3}$	0.82	−0.19	0.73	0.37	0.82	0.22	0.73	0.47
$\frac{\langle w'u'w'\rangle}{u_*^3}$	1.48	−0.15	0.91	0.24	1.48	−0.15	0.95	0.28
$P_s\frac{h}{u_*^3}$	0.86	0.43	0.73	0.94	1.15	0.03	0.98	0.37
$P_w\frac{h}{u_*^3}$	1.22	0.30	0.98	0.78	1.43	0.17	0.95	1.12
$P_d\frac{h}{u_*^3}$	1.36	1.57	0.94	1.02	1.39	1.73	0.93	1.29
$P_t\frac{h}{u_*^3}$	0.23	−0.13	0.38	1.64	0.29	−0.14	0.30	1.83
ΔS_0	1.20	0.03	0.98	0.09	1.22	−0.01	0.97	0.11
Closure	2nd				3rd			
	a	b	r^2	RMSE	a	b	r^2	RMSE
$\overline{u}/u_*$	1.1	−0.37	0.98	0.11	1.1	−0.41	0.98	0.13
$\langle\overline{u'u'}\rangle$	0.70	0.36	0.92	0.08	0.69	0.39	0.92	0.08
$\langle\overline{w'w'}\rangle$	0.60	0.43	0.95	0.03	0.60	0.42	0.96	0.03
$\langle\overline{u'w'}\rangle$	0.80	−0.09	0.92	0.02	0.77	−0.11	0.93	0.02
$\langle\overline{w'u'u'}\rangle$	0.11	−0.03	0.1	0.48	0.17	−0.03	0.19	0.42
$\langle\overline{w'w'u'}\rangle$	0.11	−0.03	0.31	0.27	0.13	0.03	0.24	0.26

model results already reported by Katul and Albertson (1998) for a 15-year old pine forest (see Table I). The regression statistics and root-mean-squared error between measurements and model calculations are quite comparable, at least for first- and second-order statistics. While this agreement is necessary for a 'working' second-order closure model, it is not sufficient. Many authors, including Katul and Albertson (1998), have demonstrated the possibility of reproducing well $\langle\overline{u}\rangle$, $\langle\overline{u'w'}\rangle$, $\langle\overline{u'u'}\rangle$, $\langle\overline{w'w'}\rangle$ without reproducing well the triple correlations. Hence,

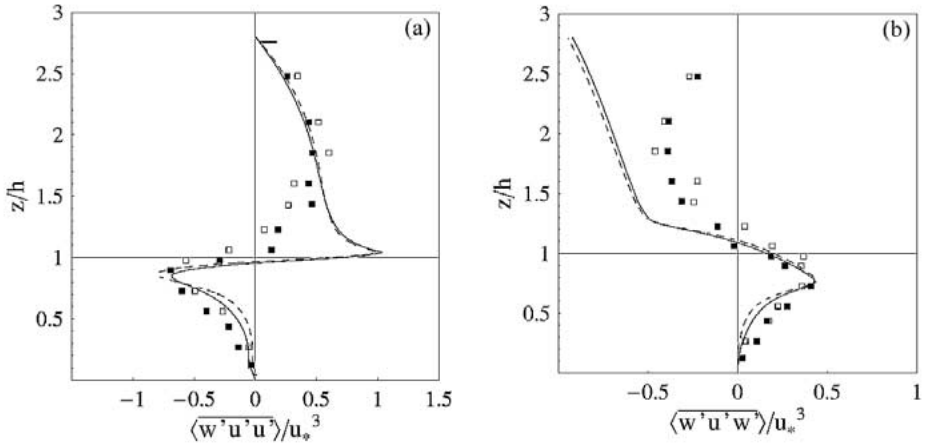

Figure 5. Comparison between measured and modelled horizontally-averaged moments with normalized height (z/h) for (a) $\langle \overline{w'u'u'} \rangle / u_*^3$, (b) $\langle \overline{w'u'w'} \rangle / u_*^3$. The solid symbols (measurements) and solid lines (model calculations) are for Re_b = 172,300 while the open symbols (measurements) and dashed lines (model calculations) are for Re_b = 116,560.

we consider next the triple correlation comparisons and also discuss them in the context of the Katul and Albertson (1998) findings.

6.2. Gradient-diffusion and triple correlation comparisons

In Figure 5, the comparison between measured and modelled triple moments ($\langle \overline{w'u'u'} \rangle$, $\langle \overline{w'u'w'} \rangle$) are shown for both Re_b. Table I presents the regression statistics between measured and modelled quantities shown in Figure 5. For reference, the triple velocity model comparisons reported by Katul and Albertson (1998) for the pine forest are also shown in Table I. Within the canopy of the flume experiment, good agreement between measured and modelled triple velocity correlation is noted. In fact, the agreement between measurements within the canopy and model calculations is by far superior to the agreement reported by Katul and Albertson (1998) for their pine forest. Just above the canopy, the agreement between measured and modelled third-order moments is inferior to that of the second-moment comparisons. However, the closure model does capture the overall shape of these profiles. It is necessary to note here that the abrupt transition from a finite (and large) drag within the canopy to a zero drag just above the canopy is likely responsible for much of the departure between measurements and model. At this transition point, not only is the drag coefficient discontinuous, the vertical gradient in the shear stress profile, which drives the closure for all triple velocity correlations, is also nearly discontinuous. How these departures between model calculations and measurements of triple correlations affect TKE and $\langle \Delta S_o \rangle$ is discussed next.

6.3. TKE BUDGET COMPARISONS

The modelled P_s, P_w, and P_t agree well with the measurements (see Table I). The agreement between measured and modelled P_s is not too surprising because P_s is primarily driven by $\langle\overline{u}\rangle$ and $\langle\overline{u'w'}\rangle$, which are constrained by the mean momentum balance. The agreement between measured and modelled P_w serves as a stronger metric for model performance, though uncertainty in our measured P_w (at least when compared to P_s) is larger. This, in part, is due to the sensitivity of measured P_w in Equation (28) to spatial sampling of time-averaged velocity and its gradients. Hence, when taken together with the previous results of Figures 4 and 5, the agreement shown here lends support to both the wake production parameterization and the weighted spatial averaging procedures employed in the measurements. The measured and modelled P_t appear to be in good agreement despite the sharp discontinuity across the canopy-top in $C_d a$. We emphasize that the measured P_t is the turbulent transport and ignores contributions from the pressure transport. Hence, a 1 : 1 comparison between measured and modelled P_t should be treated with caution, as the contribution of the pressure transport to the overall transport terms remains uncertain (Finnigan, 2000). Finally, we compared measured and modelled TKE dissipation rates and note reasonable agreement despite the primitive treatment of the dissipation term by the closure model and the uncertainty in the measurements.

6.4. NON-LOCAL MOMENTUM TRANSPORT COMPARISONS

Before presenting comparisons between measured and modelled ΔS_o, it is necessary to evaluate the accuracy of the third-order CEM and the ICEM first. This permits us to isolate errors attributed to the CEM expansion from errors attributed to gradient-diffusion approximations. To assess the CEM expansion, we show a sample comparison between measured and modelled probability density functions (pdf) for u' and w', respectively, in Figure 7. It is clear that, while some features of the measured pdf are not well reproduced by third-order CEM, the observed asymmetry is well reproduced.

A more direct test is how well CEM and ICEM reproduce the measured $\langle\Delta S_o\rangle$ profile. In Figure 8, we used the measured M_{03}, M_{30}, M_{21}, and M_{12} to compute $\langle\Delta S_o\rangle$ using the CEM and ICEM expressions and then compared these calculations to the measured $\langle\Delta S_o\rangle$ obtained from quadrant analysis. It is clear that both CEM and ICEM expressions reproduce the measured $\langle\Delta S_o\rangle$ well (see Table I). Finally, we compared the measured $\langle\Delta S_o\rangle$ with the second-order closure modelled $\langle\Delta S_o\rangle$ in Figure 9 and found reasonable agreement between second-order closure model calculations and measurements (see Table I). The next logical question is 'why do gradient-diffusion approximations to third moments correctly predict the relative contributions of ejections and sweeps to momentum transfer?'. To address this question, we consider whether the sign of $\langle\Delta S_o\rangle$ is inherently well reproduced by our second-order closure model. It is clear from our experiments, as well as

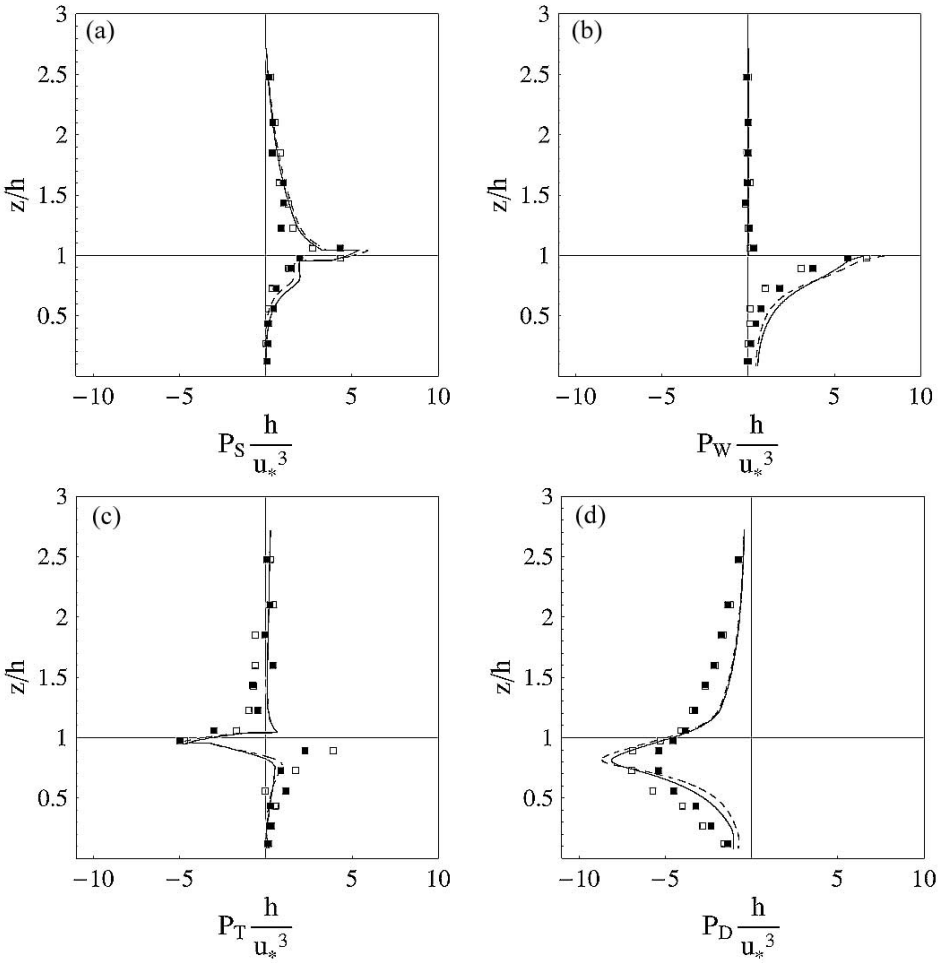

Figure 6. Comparison between measured and modelled horizontally-averaged moments with normalized height (z/h) for the components of the TKE budget (a) $P_s h/u_*^3$, (b) $P_w h/u_*^3$, (c) $P_t h/u_*^3$, and (d) $P_d h/u_*^3$. The solid symbols (measurements) and solid lines (model calculations) are Re_b = 172,300 while the open symbols (measurements) and dashed lines (model calculations) are for Re_b = 116,560.

numerous field measurements (e.g., see review in Katul and Albertson, 1998), that $\langle \Delta S_o \rangle$ appears to be positive within the canopy but approaches zero above the canopy. Upon examining Equation (26) for a finite and usually negative $\langle \overline{u'w'} \rangle$ in the CSL, the sign of $\langle \Delta S_o \rangle$ is clearly controlled by

$$\frac{1}{\sigma_u} \frac{\partial \langle \overline{u'u'} \rangle}{\partial z} - \frac{2}{\sigma_w} \frac{\partial \langle \overline{w'u'} \rangle}{\partial z}. \tag{40}$$

Noting that $\partial \langle \overline{w'u'} \rangle / \partial z$ is always negative ($= -C_d a \langle \overline{u} \rangle^2$), and that σ_u and σ_w are monotonically increasing with increasing z implies that Equation (26) will always

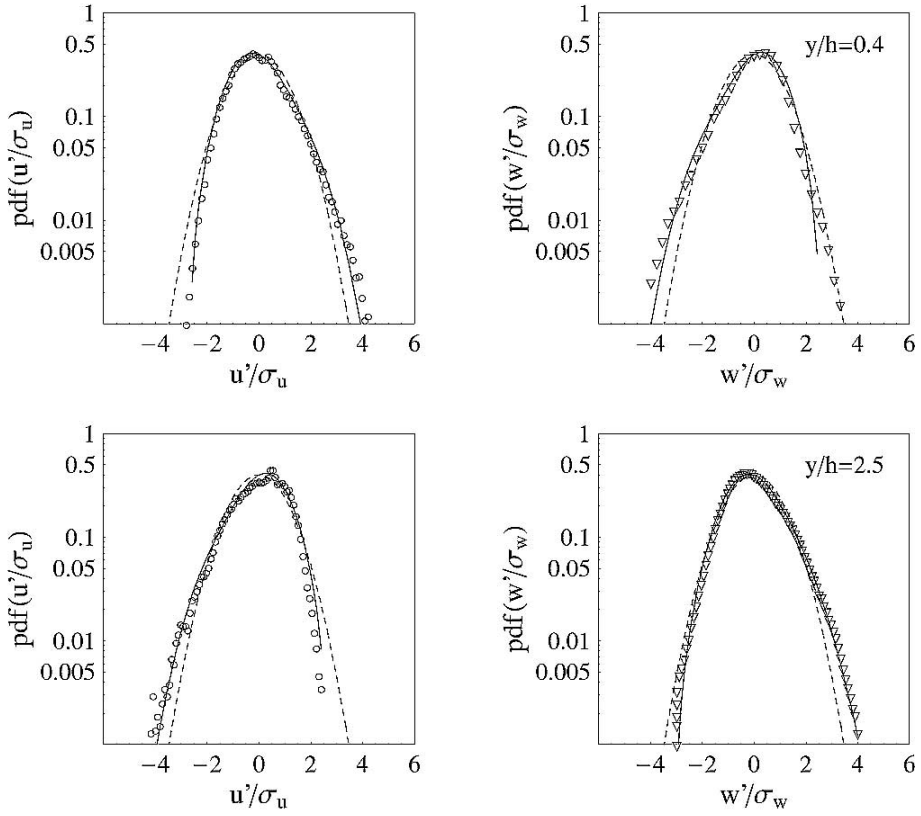

Figure 7. Comparison between measured (symbols) and CEM modelled (solid line) horizontally-averaged probability density function with normalized height (z/h). For reference, the Gaussian probability density function is also shown (dotted).

predict a positive $\langle \Delta S_o \rangle$ which is consistent with the numerous measurements (including ours) that demonstrate sweeps are more important than ejections within dense canopies (see Katul and Albertson, 1998; Katul et al., 1997). Also, in the near-constant stress layer, with $P_s \approx P_d$,

$$\frac{1}{\sigma_u}\frac{\partial \langle \overline{u'u'} \rangle}{\partial z} \approx \frac{2}{\sigma_w}\frac{\partial \langle \overline{w'u'} \rangle}{\partial z} \approx 0, \tag{41}$$

which leads Equation (26) to predict a $\langle \Delta S_o \rangle \approx 0$ again consistent with numerous experiments on rough-wall boundary layers (Raupach, 1981; Shaw et al., 1983) and the atmospheric surface layer (Katul et al., 1997). In short, the combination of ICEM and gradient-diffusion models reproduces the relative importance of ejections and sweeps on momentum transfer despite their inherent local closure assumption. Finally, we note that variations in $\langle \Delta S_o \rangle$ are strongly dependent on variations in the profiles of $\langle \overline{u'u'} \rangle$ and $\langle \overline{u'w'} \rangle$, both vary on length scales comparable to h.

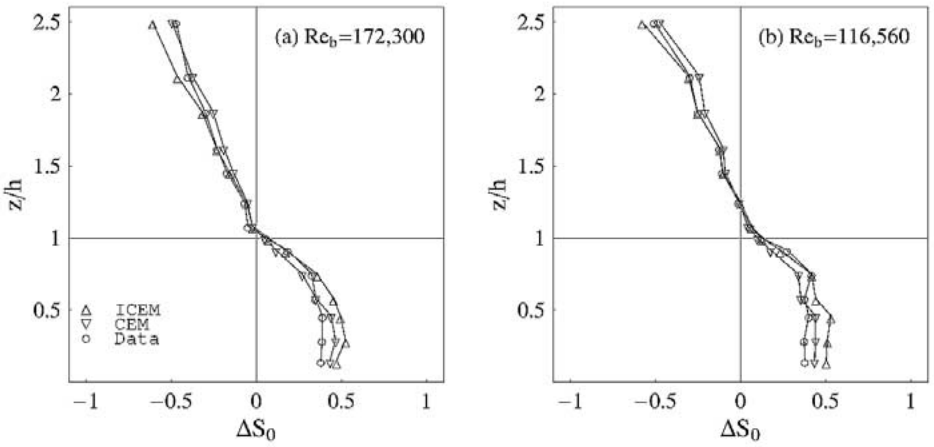

Figure 8. Comparison between measured and modelled horizontally-averaged $\langle \Delta S_o \rangle$ with normalized height (z/h)(a) Re_b = 172,300 and (b) Re_b = 116,560. The symbols are for measurements via quadrant analysis, the solid line is for the complete CEM (Equation (25)), and the dashed lines are the incomplete CEM or ICEM (Equation (26)).

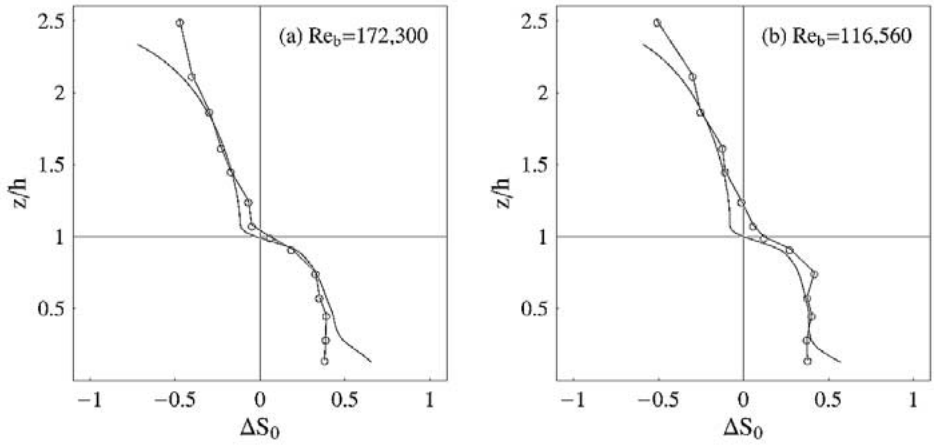

Figure 9. Comparison between measured and modelled horizontally-averaged $\langle \Delta S_o \rangle$ with normalized height (z/h)(a) Re_b = 172,300 and (b) Re_b = 116,560. The symbols (connected by a line) are for measurements via quadrant analysis, and the solid line are for the second order closure model calculations with ICEM.

7. Conclusions

Over the last two decades, several second-order closure models have been proposed and tested for CSL turbulence, each having its own strengths and weaknesses. These models share an overarching strategy in that they all employ a set of closure schemes for terms in the 'free-air' flow equations and then add extra terms to account for the canopy related processes such as drag or wake production without

altering these 'free-air' closure forms. Much of the research thrust in CSL closure models focused on these canopy modifications, their inherent time scales, and energetic partitioning.

This study did not introduce any new fundamental physics or propose alterations to existing closure schemes; rather, it proposes a new phenomenological formulation of the mixing length within the context of second-order closure scheme that takes into account the role of organized motion and effects of non-local transport within a very idealized canopy morphology: vertical rods. Also, it used independent experiments to determine the drag coefficient (C_D) and the sheltering imposed by the canopy density. For dense canopies within the CSL, the proposed effective length scale is dependent on three canonical length scales: rod diameter (d_r), the mixing layer length scale (L_{ML}), and distance from the wall (z). We showed that when this mixing length scale and C_D are combined with the second-order closure model, agreement between measured and modelled velocity moments is observed even up to triple velocity correlations within the canopy. The agreement between measured and modelled wake production and dissipation rate terms was reasonable, given the inherent uncertainty in both measurements and closure model parameterizations. Our study went further still and demonstrated a theoretical connection between the second-order closure model, cumulant expansions, and the effects of non-local momentum transport phenomena within the CSL (e.g., ejections and sweeps). The gradient-diffusion closure scheme for the triple velocity correlations appears to reproduce the relative importance of ejections and sweeps on momentum transfer reasonably well despite its inherent local closure assumption.

When these results are taken together, it appears that our predictive skill via second-order closure modelling is less limited by closure formulations and more limited by our ability to independently connect the drag coefficient and the effective mixing length scale to key morphological attributes of the canopy (at least for undisturbed flows). This is what is lacking for practical applications such as seed dispersion or biosphere-atmosphere carbon exchange. With recent advancement in laser altimetry, it is likely that detailed spatial distribution of canopy morphology, particularly roughness density, will become available. Quantifying the canonical length scale for canopy elements with multiple length scales (vis-à-vis a well defined d_r), sheltering effect, the homogeneity and isotropy of the drag coefficient for such variable roughness density requires a new concerted theoretical and experimental research effort.

Acknowledgements

The authors thank Ing. Simone Giordano and Ing. Alberto Viglione for their assistance in building the test section of the flume and collecting the experimental date, and Luca Ridolfi and Amilcare Porporato for their suggestions and support.

We acknowledge the support of the National Science Foundation (*NSF-EAR and NSF-DMS*), the Biological and Environmental Research (*BER*) Program, U.S. Department of Energy, through the Southeast Regional Center (*SERC*) of the National Institute for Global Environmental Change (*NIGEC*), and through the Terrestrial Carbon Processes Program (*TCP*) and the *FACE-FACTS* project.

References

Albertson, J. D., Katul, G. G., and Wiberg, P.: 2001, 'Relative Importance of Local and Regional Controls on Coupled Water, Carbon, and Energy Fluxes', *Adv. Water Res.* **24**, 1103–1118.

Antonia, R. A.: 1981, 'Reynolds-Number Dependence of High-Order Moments of the Streamwise Turbulent Velocity Derivative', *Boundary-Layer Meteorol.* **21**, 159–171.

Ayotte, K. W., Finnigan J. J., and Raupach R. M.: 1999, 'A Second-Order Closure for Neutrally Stratified Vegetative Canopy Flow', *Boundary-Layer Meteorol.* **90**, 189–216.

Baldocchi, D. D., Falge, E., Gu, L. , Olson, R., Hollinger, D., Running, S., Anthoni, P., Bernhofer, Ch., Davis, K., Fuentes, J., Goldstein, A., Katul, G., Law, B., Lee, X., Malhi, Y., Meyers, T., Munger, J. W., Oechel, W., Pilegaard, K., Schmid, H. P., Valentini, R., Verma, S., Vesala, T., Wilson, K., and Wofsy, S.: 'FLUXNET: A New Tool to Study the Temporal and Spatial Variability of Ecosystem-Scale Carbon Dioxide, Water Vapor and Energy Flux Densities', *Bull. Amer. Meteorol. Soc.* **82**, 2415–2435.

Batchelor, G. K.: 1967, *An Introduction to Fluid Dynamics*, Cambridge University Press, U.K., 615 pp.

Brunet, Y., Finnigan, J. J., and Raupach, M. R.: 1994, 'A Wind Tunnel Study of Air Flow in Waving Wheat: Single-Point Velocity Statistics', *Boundary-Layer Meteorol.* **70**, 95–132.

Finnigan, J.: 2000, 'Turbulence in Plant Canopies', *Annu. Rev. Fluid Mech.* **32**, 519–571.

Finnigan, J.: 2000, 'Turbulent Transport in Flexible Plant Canopies', in B. A. Hutchinson and B. B. Hicks (eds.), *The Forest-Atmosphere Interaction*, D. Reidel Publishing Co., Dordrecht, pp. 443–480.

Hanjalić, H. H.: 2002, 'One-Point Closure Models for Buoyancy-Driven Turbulent Flow', *Annu. Rev. Fluid Mech.* **34**, 321–347.

Jackson, P. S.: 1981, 'On the Displacement Height in the Logarithmic Velocity Profile', *J. Fluid Mech.* **111**, 15–25.

Katul, G. G. and Albertson, J. D.: 1998, 'An Investigation of Higher Order Closure Models for a Forested Canopy', *Boundary-Layer Meteorol.* **89**, 47–74.

Katul, G. G., and Chang, W. H.: 1999, 'Principal Length Scales in Second-Order Closure Models for Canopy Turbulence', *J. Appl. Meteorol.* **38**, 1631–1643.

Katul, G. G., Hsieh, C. I., Kuhn, G., Ellsworth, D., and Nie, D.: 1997, 'The Turbulent Eddy Motion at the Forest-Atmosphere Interface', *J. Geophys. Res.* **102**, 13409–13421.

Katul, G. G., Lai, C. T., Schafer, K., Vidakovic, B., Albertson, J. D., Ellsworth, D., and Oren, R.: 2001, 'Multiscale Analysis of Vegetation Surface Fluxes: From Seconds to Years', *Adv. Water Res.* **24**, 1119–1132.

Launder, B. E.: 1996, 'An Introduction to Single-Point Closure Methodology', in T. G. Gatski, M. Y. Hussaini, and J. L. Lumley (eds.), *Simulation and Modeling of Turbulent Flows*, Oxford University Press, Oxford, New York, pp. 243–310.

Lumley, J. L.: 1978, 'Computational Modelling of Turbulent Flows', *Adv. Appl. Mech.* **18**, 123–142.

Massman, W. J.: 1997, 'An Analytical One-Dimensional Model of Momentum Transfer by Vegetation of Arbitrary Structure', *Boundary-Layer Meteorol.* **83**, 407–421.

Massman, W. J. and Weil, J. C.: 1999, 'An Analytical One-Dimensional Second-Order Closure Model of Turbulence Statistics and the Lagrangian Timescale within and above Plant Canopies of Arbitrary Structure', *Boundary-Layer Meteorol.* **91**, 81–107.

Mellor, G.: 1973, 'Analytic Prediction of the Properties of Stratified Planetary Boundary Layer', *J. Atmos. Sci.* **30**, 1061–1069.

Meyers, T. and Paw U, K. T.: 1986, 'Testing of a Higher-Order Closure Model for Modeling Airflow within and above Plant Canopies', *Boundary-Layer Meteorol.* **37**, 297–311.

Nakagawa, H. and Nezu, I.: 1977, 'Prediction of the Contributions to the Reynolds Stress from Bursting Events in Open Channel Flows', *J. Fluid Mech.* **80**, 99–128.

Nathan, R., Katul, G. G., Horn, H. S., Thomas, S. M., Oren, R., Avissar, R., Pacala, S. W., and Levin, S. A.: 1977, 'Mechanisms of Long-Distance Dispersal of Seeds by Wind', *Nature* **418**, 409–413.

Pinard, J. P. and Wilson, J. D.: 2001, 'First- and Second-Order Closure Models for Wind in a Plant Canopy', *J. Appl. Meteorol.* **40**, 1762–1768.

Poggi, D., Porporato, A., Ridolfi, L., Albertson, J. D., and Katul, G. G.: 2004a, 'The Effect of Vegetation Density on Canopy Sub-Layer Turbulence', *Boundary-Layer Meteorol.* **111**, 565–587.

Poggi, D., Katul, G. G., and Albertson, J. D.: 2004b, 'A Note on the Contribution of Dispersive Fluxes to Momentum Transfer within Canopies', *Boundary-Layer Meteorol.* **111**, 615–621.

Pope, S. B.: 2000, *Turbulent Flows*, Cambridge University Press, U.K., 771 pp.

Raupach, M. R.: 1981, 'Conditional Statistics of Reynolds Stress in Rough-Wall and Smooth-Wall Turbulent Boundary Layers', *J. Fluid Mech.* **108**, 363–382.

Raupach, M. R.: 1988, 'Canopy Transport Processes', in W. L. Steffen and O. T. Denmead (eds.), *Flow and Transport in the Natural Environment*, Springer-Verlag, New York, pp. 95–127.

Raupach, M. R.: 1994, 'Simplified Expressions for Vegetation Roughness Length and Zero-Plane Displacement as Functions of Canopy Height and Area Index', *Boundary-Layer Meteorol.* **71**, 211–216.

Raupach, M. R. and Shaw, R. H.: 1982, 'Averaging Procedures for Flow within Vegetation Canopies', *Boundary-Layer Meteorol.* **61**, 47–64.

Raupach, M. R. and Thom, A. S.: 1981, 'Turbulence in and above Plant Canopies', *Annu. Rev. Fluid Mech.* **13**, 97–129.

Raupach, M. R., Finnigan, J. J., and Brunet, Y.: 1996, 'Coherent Eddies and Turbulence in Vegetation Canopies: The Mixing Layer Analogy', *Boundary-Layer Meteorol.* **78**, 351–382.

Shaw, R. H.: 1977, 'Secondary Wind Speed Maxima Inside Plant Canopies', *J. Appl. Meteorol.* **16**, 514–521.

Shaw, R. H. and Schumann, U.: 1992, 'Large-Eddy Simulations of Turbulent Flow above and within a Forest', *Boundary-Layer Meteorol.* **61**, 47–64.

Shaw, R. H., Tavangar, J., and Ward, D.: 1983, 'Structure of the Reynolds Stress in a Canopy Layer', *J. Clim. Appl. Meteorol.* **22**, 1922–1931.

Seginer, I., Mulhearn, P. J., Bradley E. F., and Finnigan, J. J.: 1976, 'Turbulent Flow in a Model Plant Canopy', *Boundary-Layer Meteorol.* **10**, 423–453.

Thom, A. S.: 1971, 'Momentum Absorption by Vegetation', *Quart. J. Roy. Meteorol. Soc.* **97**, 414–428.

Wilson, J. D.: 1988, 'A Second Order Closure Model for Flow through Vegetation', *Boundary-Layer Meteorol.* **42**, 371–392.

Wilson, N. R. and Shaw, R. H.: 1977, 'A Higher Order Closure Model for Canopy Flow', *J. Appl. Meteorol.* **16**, 1198–1205.

Wofsy, S. C., Goulden, M. L., Munger, J. W., Fan, S. M., Bakwin, P. S., Daube, B. C., Bassow, S. L., and Bazzaz, F. A.: 1993, 'Net Exchange of CO_2 in a Mid-Latitude Forest', *Science* **260**, 1314–1317.